

# High temperature superconductor dc SQUID micro-susceptometer for room temperature objects

M I Faley<sup>1</sup>, K Pratt<sup>2</sup>, R Reineman<sup>2</sup>, D Schurig<sup>2</sup>, S Gott<sup>2</sup>,  
C G Atwood<sup>2</sup>, R E Sarwinski<sup>2</sup>, D N Paulson<sup>2</sup>, T N Starr<sup>2</sup> and  
R L Fagaly<sup>2</sup>

<sup>1</sup> Institut für Festkörperforschung, Forschungszentrum Jülich GmbH, 52425 Jülich, Germany

<sup>2</sup> Tristan Technologies, Inc., 6185 Cornerstone Court East, Suite 106, San Diego, CA 92121, USA

Received 13 February 2004

Published 6 April 2004

Online at [stacks.iop.org/SUST/17/S324](http://stacks.iop.org/SUST/17/S324) (DOI: 10.1088/0953-2048/17/5/046)

## Abstract

We have developed a scanning magnetic microscope (SMM) with 25  $\mu\text{m}$  resolution in spatial position for the magnetic features of room temperature objects. The microscope consists of a high-temperature superconductor (HTS) dc SQUID sensor, suspended in vacuum with a self-adjusting standoff, close spaced liquid nitrogen Dewar,  $X$ – $Y$  scanning stage and a computer control system. The HTS SQUIDs were optimized for better spatial and field resolutions for operation at liquid nitrogen temperature. Measured inside a magnetic shield, the 10 pT  $\text{Hz}^{-1/2}$  typical noise of the SQUIDs is white down to frequencies of about 10 Hz, increasing up to about 20 pT  $\text{Hz}^{-1/2}$  at 1 Hz. The microscope is mounted on actively damped platforms, which negate vibrations from the environment as well as damping internal stepper motor noises. A high-resolution video telescope and a 1  $\mu\text{m}$  precision  $z$ -axis positioning system allow a close positioning of the sample under the sensor. The ability of the sensors to operate in unshielded environmental conditions with magnetic fields up to about 15 G allowed us to perform 2D mapping of the local ac and dc susceptibility of the objects.

(Some figures in this article are in colour only in the electronic version)

## 1. Introduction

SQUID magnetometers have an ultimate combination of field and spatial resolution. Scanning SQUID systems can be used, for example, for detection of weak magnetic fields generated by electronic circuits [1, 2]. Further improvement of the spatial resolution is possible with a scanning magnetic microscope (SMM), which would have a better combination of a smaller-sized SQUID pick-up loop, better sensor sensitivity and reduced distance to the object. Compared to other magnetic evaluation methods for microscopic objects, the SMM has a higher magnetic field sensitivity (see, for example, reviews in [3]) and high linearity over a dynamic range up to about 200 dB. The disadvantages of this instrument are modest spatial resolution and a requirement for a cooled sensor. The SMM is an established instrument for fundamental studies of

microscopic magnetic properties of objects placed in a liquid ( $^4\text{He}$  or  $\text{N}_2$ ) cryostat or at variable sample temperatures of objects placed in vacuum (see, e.g., [4, 5] and references therein).

Minimizing SQUID–sample separation for better field and spatial resolution becomes a problem for room temperature objects, which are placed outside the cryostat. Here we present a SMM for room temperature objects with a liquid-nitrogen-cooled SQUID sensor, suspended in vacuum with a self-adjusting standoff between the SQUID and window as an alternative to the bulky bellows mechanism [2, 6] for the adjustment of the window. Due to the submicrometre size of the bicrystal Josephson junctions the sensor can operate in magnetic fields up to about 15 G. This has allowed us to perform 2D mapping of the local ac and dc susceptibility of the objects.

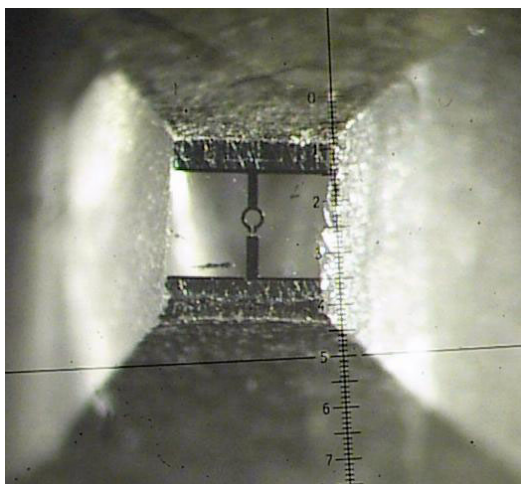


**Figure 1.** Optical image of the SQUID tip. The inner diameter of the SQUID loop is about  $50 \mu\text{m}$ .

## 2. Experimental details

The SQUID structures were prepared from  $\text{YBa}_2\text{Cu}_3\text{O}_{7-x}$  *c*-oriented films by a high oxygen pressure dc-sputtering technique [7]. The films show typical critical current densities  $J_c$  of about  $5 \times 10^6 \text{ A cm}^{-2}$  at 77 K and a transition temperature,  $T_c$ , above 91 K. The HTS Josephson junctions for the dc SQUIDs were the symmetric  $24^\circ \text{ SrTiO}_3(100)$  bicrystal junctions, which had a width of  $0.4\text{--}1 \mu\text{m}$ , a critical current density of about  $2 \times 10^4 \text{ A cm}^{-2}$ , a critical current of about  $10\text{--}50 \mu\text{A}$  and an  $I_c R_n$  product of about  $400 \mu\text{V}$  at 77 K [8].

The HTS SQUIDs were optimized for better spatial and field resolutions for operation at liquid nitrogen temperature. The sensitivity and spatial resolution depend on the sensor diameter and sample standoff distance. By fixing the inner diameter of the SQUID loop and increasing the outer diameter, one can improve the field sensitivity. But, in this case, one loses spatial resolution and the ability of the sensor to operate in high magnetic fields. The round shape of the SQUID hole was found to be optimal.

Several dc SQUIDs with a  $50 \mu\text{m}$  inner diameter of the loop and with about a  $70 \mu\text{m}$  outer diameter were prepared on a single substrate. The flux-field transfer coefficient of the SQUID was about  $500 \text{ nT}/\Phi_0$ , while the maximum flux-to-voltage transfer function was about  $60 \mu\text{V}/\Phi_0$ .

After a preliminary characterization, the SQUIDs were separated from each other by a diamond saw. The best of the SQUIDs was glued on the end of a sapphire rod and ground down from the sides to about a  $0.25 \text{ mm}^2$  tip area, as is shown in figure 1. A  $200 \text{ nm}$  thick Ag film was used to extend the contact pads of the SQUID over the edges.

The sapphire rod with the SQUID was glued inside a slotted Cu holder, which was fixed on a G-10 part containing an impedance matching circuit and a 10-pin LEMO connector. Cold leads from twisted Cu wires provided the thermal contact of the SQUID assembly with the liquid nitrogen reservoir. The step on the Cu radiation shield served as a pedestal for a fibreglass tube, which kept the SQUID–window standoff fixed at a few micrometres.

The field resolution of the sensor was measured in a  $\mu$ -metal shield and in an unshielded laboratory environment

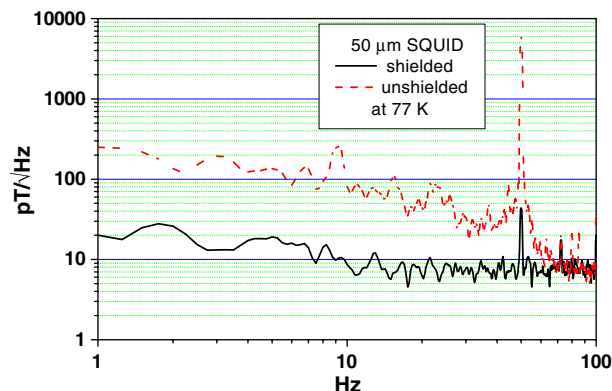


**Figure 2.** Noise of the microscope SQUID sensor both in a  $\mu$ -metal shield and unshielded. The top trace was measured in an unshielded environment.



**Figure 3.** A photograph of the complete SMM system.

(see figure 2). During the measurements the stepper motors of the positioning system were not connected. The white noise level was observed to be the same for both spectra. At frequencies below 70 Hz the signal spectrum of the unshielded sensor demonstrated mainly environmental noise.

The microscope consists of a HTS dc SQUID sensor, suspended in vacuum with a self-adjusting standoff, close spaced liquid nitrogen Dewar, *X*–*Y* scanning stage and a computer control system. The microscope is mounted on actively damped platforms, which negate the vibrations from the environment as well as damping internal stepper motor noises. In spite of these precautions, the movement of the stepper motors has increased the environmental noise detected by the sensor by about 10 times at 1 Hz. A laser profilometer, high-resolution video telescope and a  $1 \mu\text{m}$  precision *z*-axis positioning system allow us to achieve a close positioning of the sample under the sensor. The ability of the sensors to operate in unshielded environmental conditions with relatively high magnetic fields allowed measurements of the ac and dc susceptibility of the microscopic objects.

The complete SMM is shown in figure 3. The main features of this system are a thermally stabilized enclosure for the sensor and Dewar, and *xyz* scanning stages mounted on a vibrationally isolated table. The adjacent worktable houses the electronics rack, video output and controlling computer.

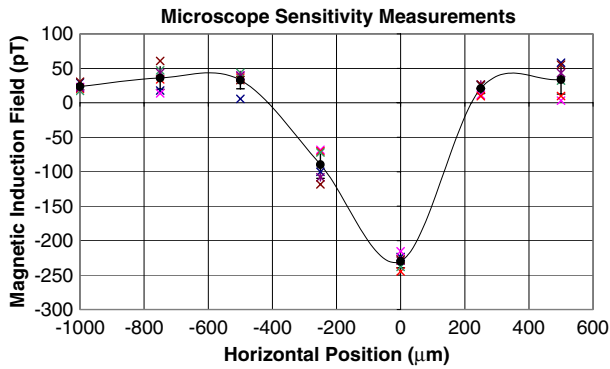


**Figure 4.** Horizontal scan above the current-carrying wires for sensitivity and spatial resolution characterization.

The sensor-to-window spacing is fixed at the factory and cannot be adjusted in the field. The positioning of the SQUID was accomplished while the device is cooled to 77 K without external intervention or adjustment. The advantages of a fixed gap system are that no user adjustments are necessary, consistent measurements from run to run can be made and there is no danger of window breakage due to unexpected Dewar warm-up.

The sensor-to-window spacing (lift-off) was verified in the evacuated and cold state using a magnetic loop calibration method. This requires horizontal scans above a loop of parallel wires carrying current in the opposite directions. By varying the physical separation of the current-carrying wires or the theoretical value for lift-off, the resulting data were fitted to a theoretical response and a value for the sensor-to-sample distance of about 400 μm was extracted.

### 3. Results

Sensitivity of a SQUID sensor can be characterized by determining the smallest field change that can be detected within a background of noise. At the closest possible spacing, a signal amplitude of 120 μV arises from a 200 Hz source current of 600 nA amplitude through the parallel wire set-up described above. A noise level of 7.5 μV was obtained in our unshielded laboratory environment. With the use of an averaging time τ of about 1 s, the lowest detectable current for that range was about 75 nA, corresponding to a magnetic field resolution of about 25 pT Hz<sup>-1/2</sup>. Measurements in

a shielded environment would yield even smaller detectable fields, as shown by the noise spectrum of the SQUID sensor in a μ-metal shield (see figure 2).

The spatial resolution of the SMM may be defined as the smallest detectable change in position of a single magnetic source, or the smallest detectable separation of multiple magnetic sources such as, for example, a set of parallel wires.

With a calibration sample placed as close to the window as possible, we may estimate the resolution of the system from the sensitivity and the maximum measured derivative of the magnetic field with respect to the position. In figure 4 we presented a result of a scan above a set of parallel wires carrying a test signal of 600 nA amplitude. From the graph in figure 4, the maximum horizontal gradient is  $\partial B/\partial x \sim 1 \text{ pT } \mu\text{m}^{-1}$ . Taking into account the field resolution of  $\delta B \sim 25 \text{ pT}$  ( $\tau \sim 1 \text{ s}$ ) in the laboratory environment, a resolution in spatial position of  $\delta x = \delta B/(\partial B/\partial x) \sim 25 \mu\text{m}$  was obtained. This value can be significantly improved for higher test currents.

To demonstrate the performance of the system, we selected an ordinary one dollar bill (figure 5(a)) as a sample. Since there is a small concentration of magnetic particles in the ink used in printing the currency, we can use the SMM to measure the remnant magnetization of the designs on the bill.

Using iterative scans of finer resolutions, a region of interest of the sample was centred about the sensor. In the following data set (figures 5(b) and (c)) we depict the letters ‘TAT’ in the word ‘States’. Signal maxima are represented by lighter shades of grey, while minima are signified by darker and darker shades. The image in figure 5(c) is a three-dimensional representation of the grey-scale bitmap presented in figure 5(b). The height of the letter ‘A’ is 4 mm. The spatial resolution of the magnetic features in figures 5(b) and (c) corresponds to the step size of this scan, which was 100 μm for both the X and Y axes. With smaller step sizes and longer averaging times, some more detail of the sample could be detected, but this would take a much longer time for the mapping.

The SMM can also be used for the evaluation of static magnetic fields, originating, for example, from magnetic recording media like magnetic tapes. The observed spatial resolution was similar to that obtained with the current-carrying wires.

### 4. Magnetic susceptibility

The system also incorporates two approaches for measuring the magnetic susceptibility of objects. The first is by attaching

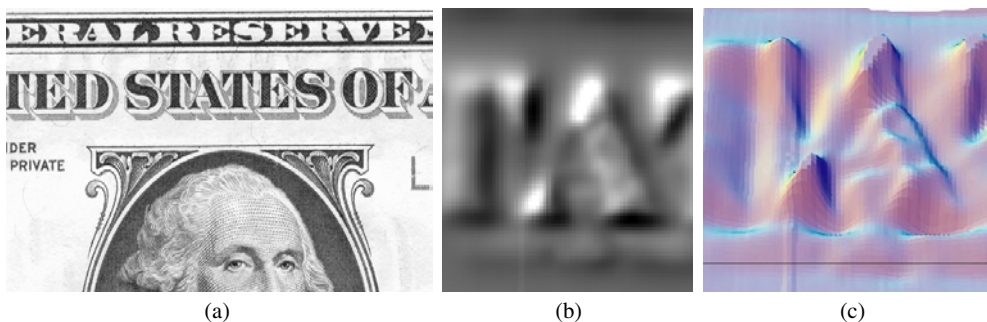


**Figure 5.** Sample of a US \$1 bill (a) used for the performance test. A grey-scale image (b) or three-dimensional representation (c) of the letters ‘TAT’ in ‘States’. The grey-scale value (b) or vertical height (c) represents the magnetic field strength.



**Figure 6.** Bottom view of the Dewar showing the excitation coil that allows us to perform susceptibility measurements. The SQUID loop is located directly above the black epoxy window.

a ring of small, powerful permanent magnets encircling the sensor tip. From symmetry, this creates a homogeneous dc magnetic field with an amplitude up to about 10 G at the sensor and the sample. By scanning a sample without a dc field and then repeating the scan with the magnet ring in place, the two data sets may be subtracted in post-processing to yield the local dc magnetic susceptibility of the sample.

There is also an excitation coil wound around a small mandrel on the Dewar tail (figure 6). This allows us to perform ac susceptibility measurements by a similar method as is described above for dc susceptibility. Running a few milliamps of current, oscillating at frequencies up to 1 kHz, through this multi-turn coil gives ac induction fields of a milligauss. By feeding sampled data into a lock-in amplifier, demodulated values can be acquired as a function of position over the sample. By running the lock-in algorithm at the same frequency with no field applied during a second scan, the two data sets may be subtracted in post-processing as they were for the dc scans. The difference in this case yields values proportional to the local ac susceptibility of the sample.

Due to the integrated ac excitation coil and special HTS SQUIDS described here, the SMM has the possibility of performing susceptibility measurements. This is advantageous in comparison with a so-called SMM with ferromagnetic antenna (see, e.g., [9] and [10]), where the ferromagnetic antenna saturates in relatively weak magnetic fields of about 1 G. The SQUID sensor used in the present work has the Josephson junction's width  $w < 1 \mu\text{m}$ . The threshold field of the flux entry in the junction  $(\pi\Phi)/(4w^2) > 15 \text{ G}$ . In the case of inhomogeneous current distribution inside the Josephson junctions this threshold field can be up to about 10 times higher.

The magnetic susceptibility option can be used for application of a SMM for non-destructive evaluation. An example of such a measurement is presented in figure 7, where the result of a 2D scan of a 1 mm wide slot in an Al plate was performed.

## 5. Summary

A novel HTS SQUID design allows the placement of a  $50 \mu\text{m}$  diameter combined pickup loop and sensor within a

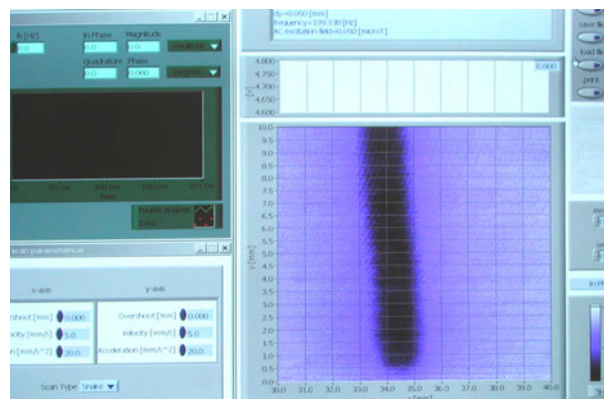


**Figure 7.** Part of the monitor image representing the computer control panel of the SMM showing the result of a scan of a 1 mm slot.

few hundred microns of the room temperature sample. This allows its operation in an unshielded environment with a large enough signal-to-noise ratio to provide useful imaging with a field resolution at the  $\sim 25 \text{ pT Hz}^{-1/2}$  level. When this sensor is combined with a novel mechanism to 'self-adjust' upon thermal cycling, a high level of reliability and utility is achieved. With a sample-to-sensor spacing of  $400 \mu\text{m}$ , an amplitude of the test signal of 600 nA and an averaging time  $\tau \sim 1 \text{ s}$  the system has demonstrated a resolution to spatial position of about  $25 \mu\text{m}$ . Anticipated future improvements in the assembly technique would be a much closer SQUID-to-window spacing. This would increase the spatial resolution by approximately an order of magnitude while maintaining the same magnetic field sensitivity.

The possibility for measuring magnetic susceptibility of microscopic objects opens up new areas of applications of the SMM, e.g. in the characterization of materials and non-destructive evaluation.

## References

- [1] Fagaly R L 1989 *IEEE Trans. Magn.* **25** 1216–8
- [2] Kirtley J R and Wikswo J P 1999 *Annu. Rev. Mater. Sci.* **29** 117–48  
Bending S J 1999 *Adv. Phys.* **48** 449–535
- [3] Anderberg J and Colclough M S 1994 *Bull. Am. Phys. Soc.* **C15** 4  
See also Anderberg J *et al* 2003 *IEEE Trans. Appl. Supercond.* **13** 231–4
- [4] Kirtley J R 2002 *Physica C* **368** 55–65
- [5] Lee T S, Chemla Y R, Dantsker E and Clarke J 1997 *IEEE Trans. Appl. Supercond.* **7** 3147–50
- [6] Fleet E F, Chatrathorn S and Wellstood F C 2001 *Rev. Sci. Instrum.* **72** 3281–90
- [7] Poppe U, Klein N, Dähne U, Soltner H, Jia C L, Kabius B, Urban K, Lubig A, Schmidt K, Hensen S, Orbach S, Müller G and Piel H 1992 *J. Appl. Phys.* **71** 5572–8
- [8] Faley M I, Poppe U, Urban K, Slobodchikov V Yu, Maslennikov Yu V, Gapelyuk A, Sawitzki B and Schirdewan A 2002 *Appl. Phys. Lett.* **81** 2406–8
- [9] Pitzjus P, Dworak V and Hartmann U 1997 *ISEC'97: Int. Conf. on Superconducting Electronics, Extended Abstracts vol 3*, ed H Koch and S Knappe (Germany: PTB Braunschweig) pp 395–8
- [10] Gudoshnikov S A, Deryuzhkina Y V, Rudenich P E, Sitnov Y S, Bondarenko S I, Shablo A A, Kalabukov A S, Snigirev O V and Seidel P 2001 *IEEE Trans. Appl. Supercond.* **11** 219–22